

Title	Core-shell ZnO nanorod lasers
Authors	Visimberga, Giuseppe;Faulkner, Colm C.;Boese, Markus;O'Dwyer, Colm
Publication date	2012-01
Original Citation	Visimberga, G., Faulkner, C. C., Boese, M. and O'Dwyer, C. (2012) 'Core-Shell ZnO Nanorod Lasers', ECS Transactions, 45(7), pp. 51-59. doi: 10.1149/1.3701525
Type of publication	Article (peer-reviewed)
Link to publisher's version	<a href="http://ecst.ecsdl.org/content/45/7/51.abstract">http://ecst.ecsdl.org/content/45/7/51.abstract</a> - 10.1149/1.3701525
Rights	© 2012 ECS - The Electrochemical Society
Download date	2024-04-18 04:45:34
Item downloaded from	<a href="https://hdl.handle.net/10468/6465">https://hdl.handle.net/10468/6465</a>



# UCC

**University College Cork, Ireland**

Coláiste na hOllscoile Corcaigh

## Core-Shell ZnO Nanorod Lasers

G. Visimberga<sup>1</sup>, C. C. Faulkner<sup>2</sup>, M. Boese<sup>2†</sup>, and C. O'Dwyer<sup>3,4\*</sup>

<sup>1</sup> *Tyndall National Institute, University College Cork, Cork, Ireland*

<sup>2</sup> *Centre for Research on Adaptive Nanostructures and Nanodevices (CRANN), Trinity College Dublin, Dublin 2, Ireland*

<sup>†</sup> *National Center for Electron Microscopy, Lawrence Berkeley National Laboratory, Berkeley, CA 94720, USA*

<sup>3</sup> *Department of Physics and Energy, University of Limerick, Limerick, Ireland*

<sup>4</sup> *Materials and Surface Science Institute, University of Limerick, Limerick, Ireland*

Room-temperature ultraviolet lasing in [0001] oriented zinc oxide nanorods grown on silicon and fused silica substrates by a simple vapor transport and condensation process. These wide band-gap semiconductor nanorods form natural laser cavities with diameters varying from 150 to 350 nm and lengths up to 10  $\mu\text{m}$ . Under optical excitation, surface-emitting lasing action was observed at 385 nm. The dielectric core-shell  $\text{Al}_2\text{O}_3@\text{ZnO}$  nanorods exhibit enhanced axial Fabry-Pérot resonating characteristics with (0001) crystal faces as mirror facets improved by a metallic reflector at one end. This metallic coating and dielectric oxide shell greatly increase near-band edge emission while reducing excitation power thresholds due to lower losses and increased optical density from improved refractive index mediated waveguiding during optical pumping.

### Introduction

There have been numerous efforts to use one-dimensional (1-D) semiconductors in field emission, field effect transistors, and optical devices due to their unique properties and potentially superior performance. ZnO has received considerable attention in recent years, including the study of diverse synthetic methods, various processing technologies, and the fabrication of versatile functional devices (1–5). The interest in developing short-wavelength semiconductor lasers has culminated in the realization of room-temperature green-blue diode laser structures with ZnSe and  $\text{In}_x\text{Ga}_{1-x}\text{N}$  as the active layers (6–8). ZnO 1-D structures, such as nanowires or nanorods, are interesting candidates for applications in optoelectronics in ultraviolet (UV) spectral region and for sensor applications due to the materials wide band gap ( $\sim 3.37$  eV), large exciton binding energy, and high surface-to-volume ratio. ZnO is suitable for blue optoelectronic applications, with ultraviolet lasing action being reported (9–11) in disordered particles, thin films and nanowires.

For wide band-gap semiconductor materials, a high carrier concentration is usually required in order to reach an optical gain that is high enough for lasing action in an electron-hole plasma (EHP) process (12). Such an EHP mechanism, which is common for conventional laser diode operation, typically requires high lasing thresholds. As an alternative to an EHP process, excitonic recombination in semiconductors is a more efficient radiative process and can allow low-threshold stimulated emission (13,14). To achieve efficient excitonic laser action at room temperature, the binding energy of the exciton must be much greater than the thermal energy at room temperature (26 meV). In

this regard, ZnO is a good candidate because its exciton binding energy is ~60 meV, substantially larger than that of ZnSe (22 meV) and GaN (25 meV). To further lower the threshold, low-dimensional compound semiconductor nanostructures have been fabricated, in which quantum size effects yield a substantial density of states at the band edges and enhance radiative recombination due to carrier confinement.

The use of semiconductor quantum well structures as low-threshold optical gain media represents a sizable advancement in semiconductor laser technology (15). Light emission from semiconductor nanowhiskers has been previously reported in GaAs and GaP systems (16,17). Stimulated emission and optical gain have also been demonstrated recently in Si and CdSe nanoclusters and their ensembles (18,19). Lasing feedback mechanism in nanorods and nanowires are often related to the formation of Fabry–Perot cavities for longitudinal modes (20), or to guided modes (21). Here, we demonstrate excitonic lasing action in ZnO nanowires with a low threshold of ~50 kW/cm<sup>2</sup> under optical excitation. We also characterize aluminium and aluminium oxide coating formation on the nanorods and end facets and correlate this dielectric-semiconductor (Al<sub>2</sub>O<sub>3</sub>@ZnO) core-shell system to high quality light emission characteristics. We investigate lasing in a vertically arranged quasi-parallel array of ZnO nanorods and randomly oriented nanowires and show that in both cases lasing is due to guided modes in individual nanorods and nanowires. The chemical flexibility and the one-dimensionality of the nanorods make them ideal miniaturized laser light sources. These short-wavelength nanolasers could have myriad applications, including optical computing, integrated nanoscale optoelectronics, photonics, information storage, and microanalysis or sensor technology.

## Experimental

In the low pressure chemical vapor deposition (CVD) growth, metallic Zn of high purity (99.999%) and an oxygen/nitrogen mixture (20% by volume of O<sub>2</sub>) were used as source materials. The growth process was carried out in a two-zone quartz reactor, shown in Fig. 1a. The first zone is for the vaporization of Zn, and Zn vapor interacts with the oxygen in the second zone, where the substrate is placed. The temperature of the Zn source material was held at 650 – 670°C, while the temperature of the substrate was 600°C, with a gas flow rate of 20 cc min<sup>-1</sup>, and a pressure in the reactor of 7 Torr. The duration of the growth process was 30 min. Silicon or silica wafers were used as the substrate. Aluminum layers 90 nm in thickness were sputtered on top of the ZnO nanorod layer. Nanorods were removed by the substrate by ultrasonication. Isolated rods were deposited on fused silica substrates (optical pumping experiments) and also on silicon substrates (CL, Raman, SEM, HRTEM).

ZnO and Al and Al<sub>2</sub>O<sub>3</sub> coated ZnO nanorods were examined using Hitachi S-4800 and SU70 field emission scanning electron microscopes (SEM). Energy dispersive X-ray analysis (EDX) was conducted using a Hitachi SU-70 FESEM operating at 10 kV equipped with an Oxford Instruments X-max 50 mm<sup>2</sup> solid-state EDX detector. Cross-sectional transmission electron microscopy (TEM) samples were prepared by scraping NWs onto a holey carbon grid and imaged using a JEOL JEM 2100F TEM operating at 200 kV. Cathodoluminescence spectra were taken using a Philips XL30 ESEM at a temperature of 4.5 K and accelerating voltage of 10 kV. Additional EDX and HRTEM were acquired using an FEI Titan 80-300 TEM operating at 300 kV after suitable sample preparation using a Carl Zeiss Auriga focused ion beam (FIB) instrument.

Raman scattering spectra were acquired using a Horiba Jobin Yvon T64000 system with excitation wavelengths of 514 nm and 406 nm. For the investigation of the emission from a single ZnO nanorod, the radiation from the sample was collected by a microscope objective passed to the entrance slit of the spectrometer through a pin hole selecting the signal from the nanorod. The image of the nanorod in the pin hole was controlled by a CCD camera. The setup is shown in detail in Fig. 5a.

## Results and Discussion

### *Growth of ZnO nanorods and nanorod arrays*

Hexagonal ZnO nanorods with a narrow diameter distribution centered at a diameter of 150-250 nm and a typical length of 3.0-3.5  $\mu\text{m}$  are produced by low pressure chemical vapour deposition (CVD) growth on silicon substrates. Figure 1b shows the array or rods that can be grown on silicon. Higher magnification examination shows several features: the nanorods all have a hexagonal cross-section and are terminated by a characteristic disk (Fig. 1c) typical of this material. For subsequent analyses, the most common flat ended nanorods (Fig. 1d) were used as crystallographic termination and cleavage planes are required to act as mirrors for the resonant laser cavity. The array of nanorods is highly oriented perpendicular to the substrate surface.

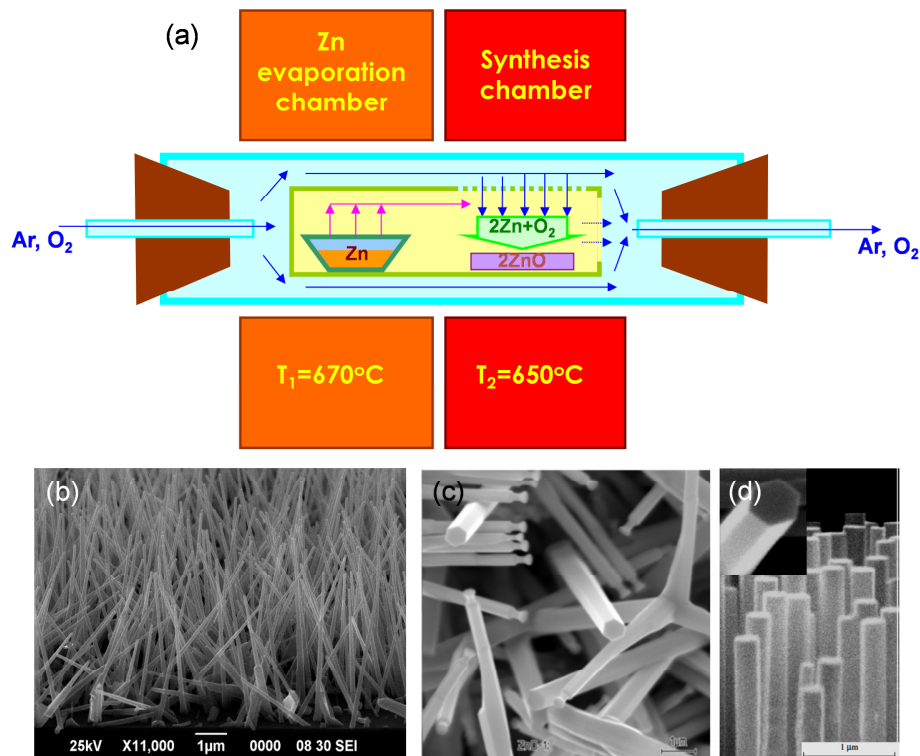


**Figure 1** (a) Schematic of the CVD system for growing ZnO nanorods layers. (b) SEM image of a layer of ZnO nanorods grown directly on silicon. (c) SEM image of nanorods with disk-shaped heads and (d) hexagonal single-crystal nanorods with flat (0001) end-facets from which optical measurements were taken.

The crystal quality of the grown nanorods were examined using a range of analytical techniques, including detailed HRTEM analyses which were compared to both cathodoluminescence and Raman scattering investigations of the crystal structure-defined

light emission under suitable optical excitation. Cathodoluminescence characterization confirms the high crystalline and optical quality ZnO nanorods. Figure 2a shows the low temperature CL spectra from a number of individual nanorods acquired at 4.5 K. The spectra show dominant free-exciton emission at  $\sim 350$  nm and importantly, do not show phonon replicas or overtones confirming good lattice quality and effective surface passivation of defects which normally results in a ‘green band’ emission. Sub-band optical emission from localized defects is either quenched or not possible due to the high crystal quality. This defect emission suppression is beneficial; we believe the quality stems from the defect-free termination of the surface facets, *i.e.* highly defined hexagonal faceting preserves the atomic structure of the terminating surface, as can be seen clearly in the HRTEM image in Figure 2b. This image shows the lattice resolution image of the ZnO nanorods edge. We see that the corresponding diffraction pattern confirms a single crystal with a [0001] growth direction.

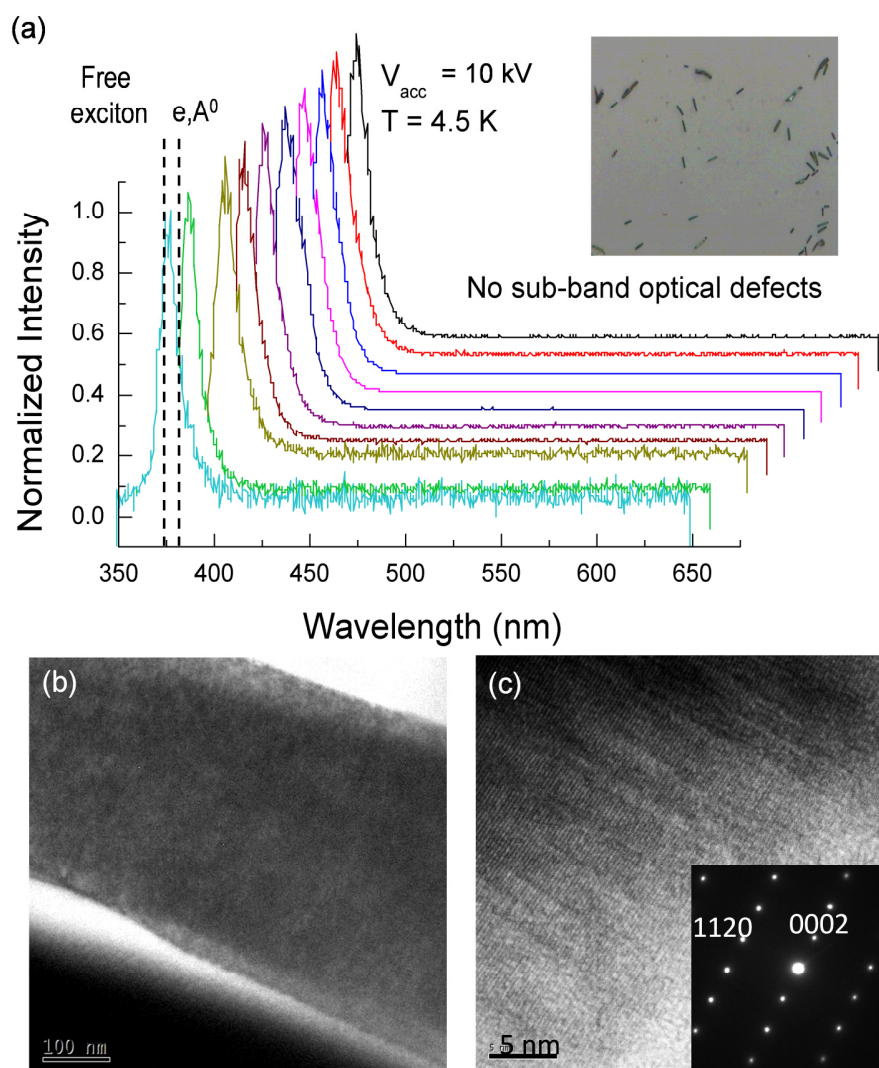


**Figure 2** (a) Cathodoluminescence spectra acquired from a range of individual nanorods shown in the inset optical image. Spectra were acquired at 4.5 K at an accelerating voltage of 10 kV. (b) HRTEM image of the edge of a ZnO nanorod and associated electron diffraction pattern.

The HRTEM image in Fig. 2b confirms a 2.36 Å spacing consistent with the interplanar spacing between two [1120 planes]; lattice spacings of 2.55 Å between two (0002) adjacent lattice planes in other 2D lattice-resolved images further prove [0001] to be the preferred growth direction for the ZnO nanorods. The striations within the image stems from thickness variations viewed in transmission so close to the edge are not stacking faults, which was confirmed by CL which is very sensitive to stacking fault and defect induced emission from 450 – 700 nm, which is featureless, confirming no structure related sub-band optical defect contributions.

Sensitive optical characterization of the nanorods crystal structures were also acquired using Raman scattering spectroscopy. The spectra of the ZnO nanorods were taken at 514 nm and also in near resonance condition at 406 nm excitation, are shown in Fig. 3. The spectra demonstrate a high quality wurtzite crystal structure. Wurtzite ZnO belongs to the  $C_{6v}$  space group ( $P6_3mc$ ). According to group theory, the corresponding zone center optical phonons have the following symmetry modes:  $A_1 + 2B_1 + E_1 + 2E_2$ . The  $A_1 + E_1 + 2E_2$  modes are Raman active, while  $2B_1$  phonons are silent. The low frequency  $E_2$  mode is predominantly associated with the non-polar vibration of the heavier Zn sub-lattice, while the high-frequency  $E_2$  mode predominantly involves the displacements of lighter oxygen atoms. The  $A_1$  and  $E_1$  modes are split into LO and TO components. All Raman active phonon modes, including LO modes, are clearly identified in the measured spectra.

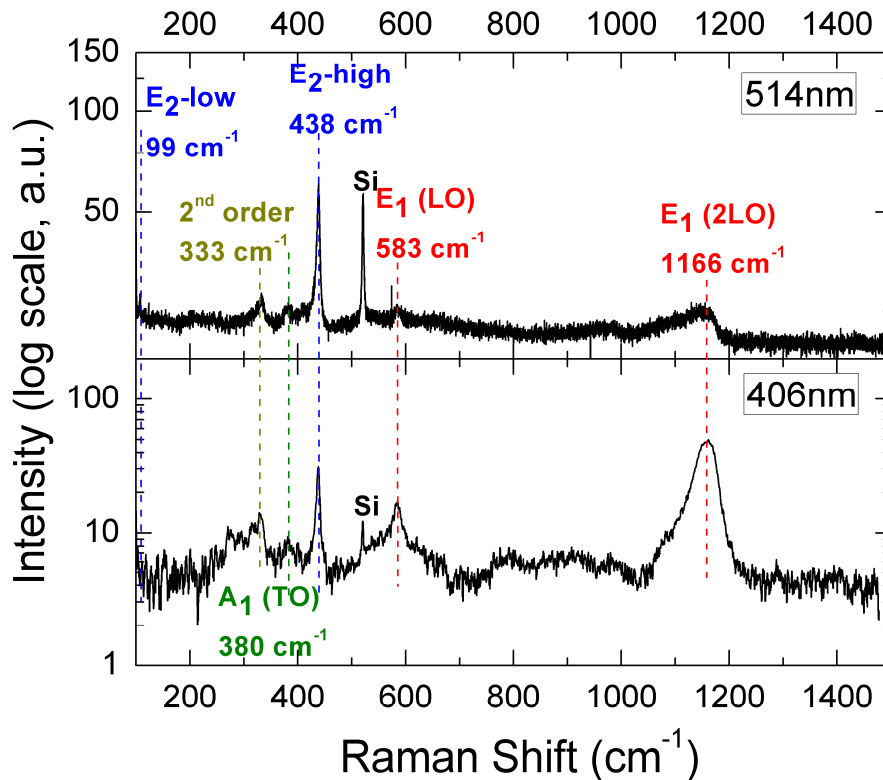


**Figure 3** Raman scattering spectra from a single ZnO nanorods acquired using excitation wavelengths of 514.5 nm and 406 nm (near resonance).

The peak at 331  $\text{cm}^{-1}$  is attributed to second order Raman processes involving acoustic phonons (22). Analysis of the spectra identifies several key indications of high crystal quality. The emission that comes from two-phonon density of states (DOS)



typically found from 500 to 700  $\text{cm}^{-1}$  (23) is very weak. Secondly, the  $E_2$  (high) mode peak has a line-width of 6.2  $\text{cm}^{-1}$ , while the line-width of the  $E_2$  (low) mode is only 0.8  $\text{cm}^{-1}$ , which is an improvement over values reported for high-quality ZnO bulk crystals (24). Thirdly, the position of the  $E_2$  (high) mode, described above, corresponds to the phonon of a bulk ZnO crystal, indicating that the nanorods are essentially strain-free. In resonance condition, this confirmed by negligible increase in intensity of this mode compared to excitation at 514 nm, and further confirmed by the observation of a large intensity increase for the  $E_1$  2LO mode at resonance, indicative of high electron-phonon coupling.

#### *Dielectric coating of ZnO nanorods and end facet mirror metallization*

The nanorods were coated after CVD growth with a 90 nm thick layer of aluminum. The aluminum was deposited over the nanorods while they were still attached to the growth substrate so that a preferential coating of one end facet of the crystalline rod was feasible, while also coating the outside of the rod. This gave ZnO nanorods with a nominal shell of aluminum which oxidized to  $\text{Al}_2\text{O}_3$ . Figure 4a show SEM images at 10 kV of the  $\text{Al}_2\text{O}_3$ @ZnO core-shell nanorods. Here, the lower atomic weight and thinner coating material appears more transparent than the central nanorod. Electron energy loss measurements confirm that metallic aluminium remained at the interface between the end facet and the  $\text{Al}_2\text{O}_3$ .

Dielectric  $\text{Al}_2\text{O}_3$  forms a coating around the resonating waveguide cavity reducing optical losses due to changes in the index contrast. Quantitative EDX measurements of a single nanorods confirms they are grown with stoichiometric ZnO composition (within a precision of 1 at%). High resolution EDX measurements from TEM analyses of the core-shell rods, shown in Fig. 4b confirm  $\text{Al}_2\text{O}_3$  formation on the walls of the nanorods, and this was confirmed by HRTEM measurements (Fig. 4c) where a  $\sim 80$  nm coating of  $\text{Al}_2\text{O}_3$  is found. Unlike the end mirror facet, where a thin metallic Al layer remains at the ZnO interface, the sidewall Al deposit has completely oxidized. As the molar volume of  $\text{Al}_2\text{O}_3$  is 2.57 times that of Al, the likely thickness of the sidewall deposit at the region of measurement is  $\sim 30$ -35 nm in this case.

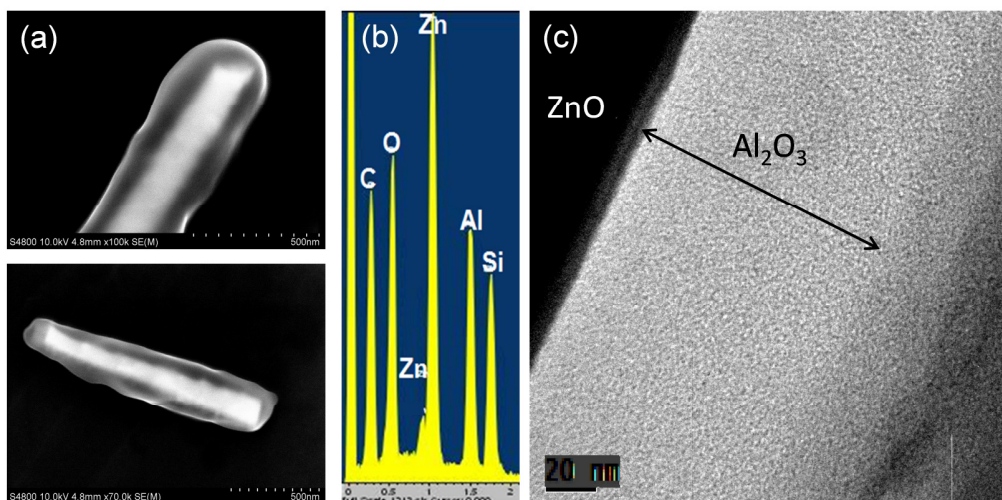


**Figure 4** (a) SEM images of the core-shell nanorods highlighting the dielectric  $\text{Al}_2\text{O}_3$  coating over the ZnO nanorods. (b) HREDS measurement of the  $\text{Al}_2\text{O}_3$  coating acquired during the acquisition of (c), a HRTEM image of the amorphous  $\text{Al}_2\text{O}_3$  layer on the nanorods sidewall.

### *Fabry-Pérot resonator cavity laser emission from nanorods*

Emission from as-made individual nanorods coated with dielectric and having a metallized end facet mirror, was investigated by considering the nanorod as a waveguide to promote optical pumping. The nanorod forms a Fabry-Pérot resonating cavity using the metallized end facet and the opposite (0001) crystal facet, of the single-crystal rod as mirrors.

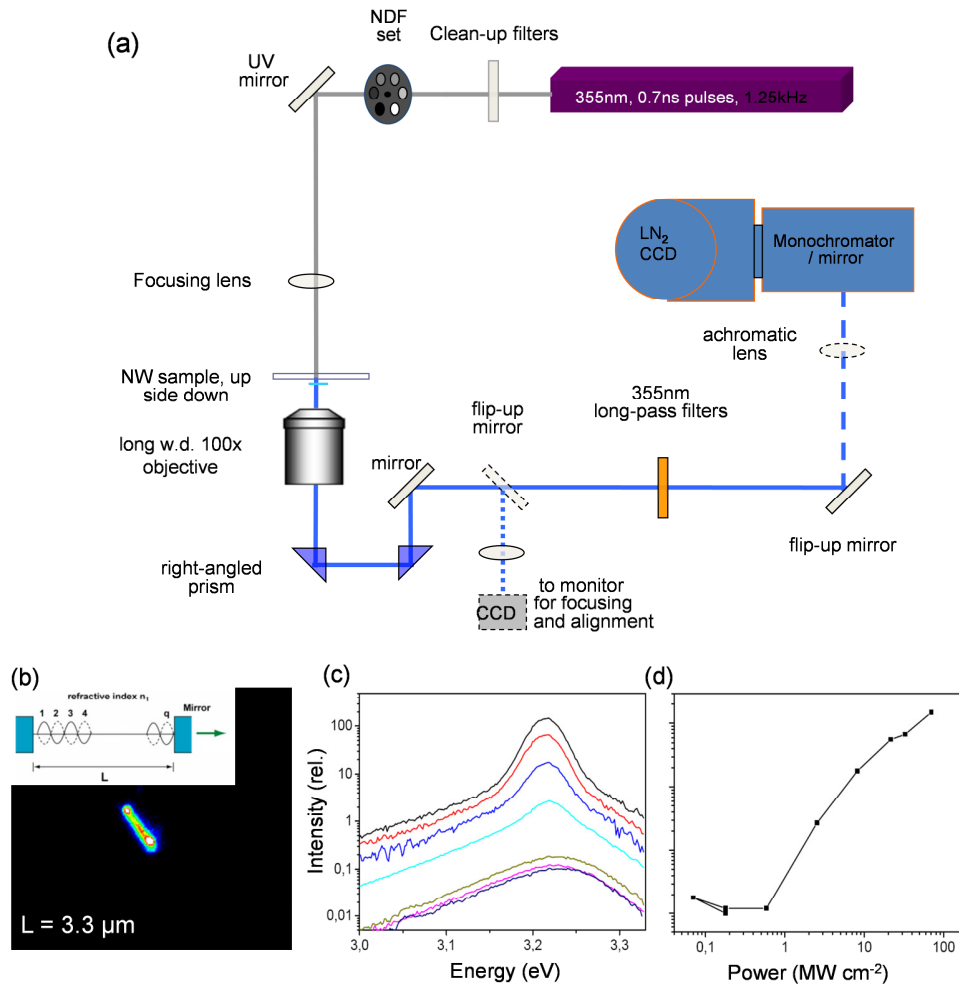


**Figure 5** (a) Schematic arrangement for the optical pumping setup for Raman scattering and emission profile characterization. (b) CCD image of the emission from a single core-shell ZnO nanorods as a resonating laser cavity. (c) Laser emission profile for a ZnO nanorod as a function of optical pump power. (v) The integrated emission peak intensity plotted as a function of optical pump power.

Figure 5b shows the signal seen through the optical microscope where clear waveguiding occurs with the most intense emission noted at the end facets of the nanorods laser. In this image, the upper end of the rod is the light injection point, through the semi-transparent mirror. The high intensity emission at the lower end of the rod is where intense lasing is found. The nanorods were perfectly levelled prior to acquisition of intensity maps. In the absence of any fabricated mirrors, we observed lasing action in the core-shell ZnO nanorods during the evolution of the emission spectra with increasing



pump power. At low excitation intensity, the spectrum consists of a single broad spontaneous emission peak (Fig. 5c) with a full width at half maximum of ~16 nm. This spontaneous emission is ~150 meV below the band gap (3.37 eV) and is generally ascribed to the recombination of excitons through an exciton-exciton collision process, where one of the excitons radiatively recombines to generate a photon (9-12). As the pump power increases, the emission peak narrows because of the preferential amplification of frequencies close to the maximum of the gain spectrum. The spectrum in Fig. 5c confirms resonator cavity lasing action with peak emission occurring at 384 nm (3.22 eV) with increased pumping power. When the excitation intensity exceeds a threshold  $\sim 50 \text{ kW cm}^{-2}$  (Fig. 5d), sharp peaks emerge in the emission spectra. The line-widths of these peaks are  $\sim 5 \text{ nm}$ , which are  $\sim 3$  times smaller than the line-width of the spontaneous emission peak below the threshold. Above the threshold, the integrated emission intensity increases rapidly with the pump power (Fig. 5d).

The integral excitation of the ZnO nanorod ensemble with 10 ns laser pulses at 4.5 K results in the emergence of narrow peaks in the emission spectrum at excitation power densities exceeding  $0.17 \text{ MW cm}^{-2}$ . These peaks increase dramatically with further increasing pump power. The narrow line-width (4-5 meV) and the rapid increase of the emission intensities of the peaks indicate that lasing occurs. The peaks represent a superposition of lasing modes from different nanorods. It is known that  $\text{Al}_2\text{O}_3@\text{ZnO}$  nanorods act both as the laser resonator for guided modes and as a gain medium for stimulated emission (21). The lasing emission wavelength is defined by the guided modes of the nanorod, which depends on its geometry.

The number and the spectrum of lasing modes fit well the expected resonance spectrum of a  $3.3 \mu\text{m}$  long nanorods with a diameter of 225 nm calculated by solving numerically the Helmholtz equation, taking into account the anisotropy of both index of refraction and gain as well as the material dispersion (25). A monotonous shift of the modes to higher photon energies occurs with increasing the excitation power density, which results from the increase of carrier density. The lasing modes show characteristic onset and saturation with increasing the excitation power density for a given cavity length. Additional lasing modes appear successively on the low energy (higher wavelength) side of the spectra as the optical pumping power is increased while previously dominating modes vanish (Fig. 5c). The lasing modes decrease in their intensity at high excitation densities, as soon as additional lasing modes appear on the low energy side, draining higher energy modes of a large density of e-h pairs (21). Furthermore, at high excitation densities the gain is red-shifted due to bandgap renormalization, and therefore modes with longer wavelength are preferentially amplified (26).

## Conclusions

This study demonstrates that a high optical quality vertically arranged nearly parallel array of ZnO nanorods and randomly oriented nanowires grown by low pressure chemical vapor deposition (CVD) on silica and silicon substrates. The lasing modes in individual nanorods display successive onset and saturation with low lasing thresholds with very high quality emission and spectral purity. The dielectric core-shell  $\text{Al}_2\text{O}_3@\text{ZnO}$  nanorods exhibit enhanced axial Fabry-Pérot resonating characteristics with (0001) crystal faces as mirror facets improved by a metallic reflector at one end. This metallic coating and dielectric oxide shell greatly increase near-band edge emission while reducing excitation power thresholds due to lower losses and increased optical density from improved refractive index mediated waveguiding during optical pumping. At high

excitation densities the gain is red-shifted due to bandgap renormalization, and therefore modes with longer wavelengths are preferentially amplified. Individual guided modes are resolved also in arrays of ZnO nanorods, provided that the geometrical parameters of the nanorods are known.

### Acknowledgments

This work was supported by EU Framework 6 Network of Excellence PhOREMOST and Science Foundation Ireland under grant No. 07/SK/B1232a. Part of this work was conducted under the framework of the INSPIRE programme, funded by the Irish Government's Programme for Research in Third Level Institutions, Cycle 4, National Development Plan 2007-2013.

### References

- (1) C. Soci, A. Zhang, B. Xiang, S. A. Dayeh, D. A. R. Aplin, J. Park, X. Y. Bao, Y. H. Lo, and D. Wang, *Nano Lett.* **7**, 1003 (2000).
- (2) J. I. Sohn, W. K. Hong, M. J. Lee, T. Lee, H. Sirringhaus, D. J. Kang, and M. E. Welland, *Nanotech.*, **20**, 505202 (2009).
- (3) J. S. Lee, M. S. Islam, and S. Kim, *Nano Lett.*, **6**, 1487 (2006).
- (4) J. B. K. Law, and J. T. L. Thong, *Nanotech.*, **18**, 055601 (2007).
- (5) J. Nayak, J. Kasuya, A. Watanabe, and S. Nozaki, *J. Phys: Condens. Matter*, **20**, 195222 (2000).
- (6) D. A. Gaul, W. S. Rees Jr., *Adv. Mater.* **12**, 935 (2000).
- (7) M. A. Hasse, J. Qui, J. M. De Puydt, H. Cheng, *Appl. Phys. Lett.* **59**, 1272 (1991).
- (8) S. Nakamura *et al.*, *Jpn. J. Appl. Phys.* **35**, L74 (1996).
- (9) H. Cao *et al.*, *Phys. Rev. Lett.* **84**, 5584 (2000).
- (10) D. M. Bagnall *et al.*, *Appl. Phys. Lett.* **70**, 2230 (1997).
- (11) P. Yu *et al.*, *J. Cryst. Growth* **184/185**, 601 (1998).
- (12) C. Klingshirn, *J. Cryst. Growth* **117**, 753 (1992).
- (13) Y. Kayamura, *Phys. Rev. B* **38**, 9797 (1988).
- (14) W. Wegscheider *et al.*, *Phys. Rev. Lett.* **71**, 4071 (1993).
- (15) D. Mehus, D. Evans, *Laser Focus World* **31**, 117 (1995).
- (16) K. Haraguchi *et al.*, *Appl. Phys. Lett.* **60**, 745 (1992).
- (17) X. Duan, Y. Huang, Y. Cui, J. Wang, C. M. Lieber, *Nature* **409**, 66 (2001).
- (18) V. I. Klimov *et al.*, *Science* **290**, 314 (2000).
- (19) L. Pavesi, L. D. Negro, C. Mazzoleni, G. Franzo, F. Priolo, *Nature* **408**, 440 (2000).
- (20) M.H. Huang, S. Mao, H. Feick, H. Yan, Y. Wu, H. Kind, E. Weber, R. Russo, P. Yang, *Science* **292**, 1897 (2001).
- (21) H. Zhou, M. Wissinger, J. Fallert, R. Hauschild, F. Stelzl, C. Klingshirn, H. Kalt, *Appl. Phys. Lett.* **91**, 181112 (2007).
- (22) M. Rajalakshmi, A.K. Arora, B.S. Bendre, S. Mahamuni, *J. Appl. Phys.* **87**, 2445 (2000).
- (23) J. Serrano, A.H. Romero, F.J. Manjon, R. Lauck, M. Cardona, A. Rubio, *Phys. Rev. B* **69**, 094306 (2004).
- (24) J. Serrano, F.J. Manjon, A.H. Romero, F. Widulle, R. Lauck, M. Cardona, *Phys. Rev. Lett.* **90**, 055510 (2003).
- (25) R. Hauschild, H. Kalt, *Appl. Phys. Lett.* **89**, 123107 (2006).
- (26) C. Klingshirn, *Semiconductor Optics*, 3rd edn. (Springer, Berlin, 2007)